



**HAL**  
open science

## Impact of Mn addition on catalytic performance of Cu/SiBEA materials in total oxidation of aromatic volatile organic compounds

Anna Rokicińska, Patrycja Majerska, Marek Drozdek, Sebastian Jarczewski, Laetitia Valentin, Jianhong Chen, Adam Slabon, Stanislaw Dzwigaj, Piotr Kuśtrowski

### ► To cite this version:

Anna Rokicińska, Patrycja Majerska, Marek Drozdek, Sebastian Jarczewski, Laetitia Valentin, et al.. Impact of Mn addition on catalytic performance of Cu/SiBEA materials in total oxidation of aromatic volatile organic compounds. *Applied Surface Science*, 2021, 546, pp.149148. 10.1016/j.apsusc.2021.149148 . hal-03170296

**HAL Id: hal-03170296**

**<https://hal.sorbonne-universite.fr/hal-03170296>**

Submitted on 16 Mar 2021

**HAL** is a multi-disciplinary open access archive for the deposit and dissemination of scientific research documents, whether they are published or not. The documents may come from teaching and research institutions in France or abroad, or from public or private research centers.

L'archive ouverte pluridisciplinaire **HAL**, est destinée au dépôt et à la diffusion de documents scientifiques de niveau recherche, publiés ou non, émanant des établissements d'enseignement et de recherche français ou étrangers, des laboratoires publics ou privés.

# **Impact of Mn addition on catalytic performance of Cu/SiBEA materials in total oxidation of aromatic volatile organic compounds**

Anna Rokicińska<sup>a</sup>, Patrycja Majerska<sup>a</sup>, Marek Drozdek<sup>a</sup>, Sebastian Jarczewski<sup>a</sup>, Laetitia Valentin<sup>b</sup>, Jianhong Chen<sup>c</sup>, Adam Slabon<sup>c</sup>, Stanislaw Dzwigaj<sup>b,\*</sup>, Piotr Kuśtrowski<sup>a,\*</sup>

<sup>a</sup>*Faculty of Chemistry, Jagiellonian University, Gronostajowa 2, 30-387 Kraków, Poland*

<sup>b</sup>*Laboratoire de Réactivité de Surface, Sorbonne Université-CNRS, UMR 7197, 4 place Jussieu, Case 168, F-75252, Paris, France*

<sup>c</sup>*Department of Materials and Environmental Chemistry, Stockholm University, Svante Arrhenius väg 16 C, 106 91 Stockholm, Sweden*

## **Abstract**

Dealuminated BEA zeolite (SiBEA) was chosen as a support of metal oxide(s) phase for catalytic combustion of volatile organic compounds (VOCs). Copper and/or manganese oxide(s) were deposited at various Cu/Mn molar ratios. Factors influencing the catalytic activity were found by chosen physicochemical methods, including XRD, XRF, low-temperature N<sub>2</sub> adsorption, FT-IR, UV-Vis-DRS, STEM-EDX, XPS and H<sub>2</sub>-TPR. Depending on the chemical composition, CuO, (Cu<sub>x</sub>Mn<sub>3-x</sub>)<sub>1-δ</sub>O<sub>4</sub>, Cu-doped Mn<sub>3</sub>O<sub>4</sub> or Mn<sub>2</sub>O<sub>3</sub> was formed as the dominant phase. The active phase particles were located mainly in the interparticle voids of the zeolite support. SiBEA gained Lewis acid sites after the introduction of the metal oxide phase, especially in the case of CuO deposition. The presence of copper in the catalytic system resulted in enhanced reducibility of the active phase, and in a consequence in high catalytic activity in the total oxidation of aromatic VOCs, which proceeds according to the Mars-van Krevelen mechanism. After the introduction of Mn, the co-existence of different valence forms was found due to the redox equilibrium:  $\text{Cu}^{2+} + \text{Mn}^{3+} = \text{Cu}^{+} + \text{Mn}^{4+}$ .

---

\* Corresponding author. Tel: +48 12 6862415. E-mail: piotr.kustrowski@uj.edu.pl (Piotr Kuśtrowski)

\* Corresponding author. Tel: +33 144272113. E-mail: stanislaw.dzwigaj@upmc.fr (Stanislaw Dzwigaj)

Definitely, the addition of Mn to Cu/SiBEA increased the number of available surface vacancies and had a beneficial effect on the catalytic performance.

**Keywords:** catalytic combustion; volatile organic compounds; copper-containing catalysts; manganese-containing catalysts; BEA zeolite

## 1. Introduction

Many various technologies for the elimination of volatile organic compounds (VOCs), including adsorption, absorption and chemical transformation, have been developed because of the harmful nature of these organic pollutants [1]. However, the most efficient and economical way to remove VOCs emitted to the atmosphere at low concentrations seems to be catalytic combustion. This method allows for complete decomposition of VOCs already at low temperatures, therefore it does not lead to the formation of secondary impurities (such as NO<sub>x</sub> or dioxins) [1,2]. Due to a large variety of compounds classified as VOCs, different types of catalysts are used in the catalytic combustion. They usually contain an active phase based on precious metals or transition metal oxides. Noble metal-containing catalysts (e.g. Pt, Pd, Rh, Au, Ag) are extremely active in the total oxidation of VOCs even at low temperatures [3,4]. A disadvantage of these materials is, however, a high price of production and sensitivity to poisoning. Alternative metal oxide-based catalysts are much cheaper and stable, but exhibit lower efficiency compared to the noble metal-containing materials [5]. The most commonly used oxide systems for the total oxidation of VOCs are: CuO [6,7], MnO<sub>x</sub> [8,9], Cr<sub>2</sub>O<sub>3</sub> [10], NiO [11,12], Fe<sub>2</sub>O<sub>3</sub> [13,14] and Co<sub>3</sub>O<sub>4</sub> [15-17]. Two-component catalysts containing Co-Pt [18,19], Co-Ce [20,21], Co-Mn [22,23], Cu-Mn [24,25], Mn-Ce [26,27], Cu-Ce [28,29] or Ni-Mn [30] were also described in the literature. They often showed higher catalytic activity compared to that observed for individual components. This beneficial effect is related to

enhancement of mobility of lattice oxygen and/or facilitating the transport of electrons on the surface of catalyst.

Manganese was frequently added as the promoter of active phase for the VOCs combustion. It was found that its presence improves redox properties of a resulting oxide system. This effect is associated with the specific electronic configuration ( $[\text{Ar}] 3d^5 4s^2$ ), which opens up the possibility of creating oxide systems with Mn atoms at different oxidation states, including  $\text{MnO}$ ,  $\text{Mn}_3\text{O}_4$ ,  $\text{Mn}_2\text{O}_3$ , and  $\text{MnO}_2$  [31]. Depending on the type of support the catalytic activity of  $\text{MnO}_x$  in the total oxidation of VOCs changes in the order:  $\gamma\text{-Al}_2\text{O}_3 > \text{SiO}_2 > \text{TiO}_2$  [32]. Furthermore, Santos et al. [33] revealed a relationship between redox properties and catalytic activity of  $\text{MnO}_x$ . Easier reducible  $\text{Mn}_3\text{O}_4$  shows a significantly better catalytic performance than  $\text{Mn}_2\text{O}_3$  or  $\text{MnO}_2$  with strongly bound lattice oxygen [4,31,34,35]. This suggests that the VOCs combustion over the  $\text{MnO}_x$  catalysts takes place according to the Mars van Krevelen mechanism, i.e. an organic molecule is first oxidized by a lattice oxygen, which is then supplemented by gaseous  $\text{O}_2$  [9]. Therefore, the availability and reactivity of surface oxygen species have a significant impact on the activity of  $\text{MnO}_x$  [4].

Mixed Cu-Mn oxides in bulky form [36-40] as well as deposited on various inorganic supports (e.g.  $\text{Al}_2\text{O}_3$  [41-43],  $\text{TiO}_2$  [43],  $\text{ZrO}_2$  [43] or mesoporous MCM-41 silica [44]) were tested as catalysts in the total oxidation of aromatic VOCs. Wang et al. [41] found that appropriate interaction between Cu and Mn introduced onto an  $\text{Al}_2\text{O}_3$  surface, which is influenced by a Cu/Mn molar ratio, results in enhanced activity. The highest conversions of toluene were achieved over the catalyst with the Cu/Mn molar ratio of 0.66. However, the optimal value of this parameter determined by Kim et al. [45] for the same type of the support was 1.3. The observed differences were most likely related to the dispersion of active phase affecting the formation of various surface Cu-Mn species. On the other hand, the co-existence of Cu and Mn leads to an appearance of large number of surface defects, which together with

increasing amount of active components enhance the catalytic performance in the benzene combustion [36].

The aim of this work is to discuss the catalytic performance of individual Cu and Mn oxides as well as bimetallic oxide systems with various Cu/Mn ratios deposited on the surface of dealuminated form of BEA zeolite (SiBEA) in the total oxidation of toluene. SiBEA was selected as the support due to its stability and presence of relatively wide channels which enable homogeneous distribution of the active phase over the whole surface (both inner and external) and possibility of work at elevated temperatures (without coking which would be intensified by the presence of Brønsted acid sites). In order to better understand the influence of properties of catalysts on their activity, a wide physicochemical characterization was performed, including determination of bulk and surface composition, phase composition, porosity, acidity, reducibility as well as the chemical nature and dispersion of the metal oxide active phase. The characterization measurements were also carried out for the materials after the catalytic process, proving that the reaction follows the Mars-van Krevelen mechanism, and the coexistence of  $\text{Cu}^+/\text{Cu}^{2+}$  and  $\text{Mn}^{3+}/\text{Mn}^{4+}$  pairs within one spinel structure allows for an increase in oxygen mobility, as well as a significant improvement in catalytic activity and stability.

## **2. Experimental**

### **2.1. Catalyst preparation**

Before the introduction of the active phase, the parent tetraethylammonium BEA (TEABEA) zeolite was dealuminated by treatment in a nitric acid solution ( $13 \text{ mol L}^{-1}$ ) at  $80 \text{ }^\circ\text{C}$  for 4 h, washed several times with distilled water and dried at  $95 \text{ }^\circ\text{C}$  overnight. Then, the obtained siliceous BEA zeolite (SiBEA) with atomic Si/Al ratio of ca. 1000 was contacted with an aqueous solutions of copper nitrate ( $\text{Cu}(\text{NO}_3)_2 \times 6 \text{ H}_2\text{O}$ ), copper nitrate ( $\text{Cu}(\text{NO}_3)_2 \times 6$

H<sub>2</sub>O) with manganese nitrate (Mn(NO<sub>3</sub>)<sub>2</sub> x 6 H<sub>2</sub>O) or manganese nitrate (Mn(NO<sub>3</sub>)<sub>2</sub> x 6 H<sub>2</sub>O) with appropriate concentration of Cu and Mn (1 g of zeolite in 200 mL of solution) and stirred at 25 °C for 24 h. The concentrations of the metals salts were changed in such a way that from 2 to 10 wt % metal loading in the final catalysts obtained. Subsequently, the suspension was transferred to an evaporator and stirred under vacuum of a water pump at 60 °C until water was removed. The samples calcined at 550 °C for 3 h in air were labeled C<sub>x</sub>Mn<sub>y</sub>SiBEA, where *x* refers to Cu wt % content, and *y* refers to Mn wt % content in the prepared solid.

## 2.2. Characterization

Chemical composition of samples was determined by X-ray fluorescence (XRF) using an ARL Quant'x (Thermo Scientific) spectrometer.

X-ray diffraction (XRD) patterns were collected in a D2 Phaser (Bruker) diffractometer with a CuK $\alpha$  X-ray radiation ( $\lambda = 1.54056$  nm) in a  $2\theta$  range of 5-90° with a step of 0.02°.

UV-vis-DR spectra were recorded at ambient atmosphere on a Cary 5000 Varian spectrometer equipped with a double integrator with polytetrafluoroethylene as a reference.

Textural properties of the materials were determined by low-temperature adsorption of nitrogen at -196 °C using a Micromeritics ASAP 2020 sorptometer. Before the measurements, samples were outgassed at 250 °C for 5 h under vacuum. Specific surface areas ( $S_{\text{BET}}$  and  $S_{\text{Langmuir}}$ ) were calculated using the Brunauer-Emmett-Teller (BET) and Langmuir theory, respectively. Micropore volumes ( $V_{\text{micro}}$ ) were determined using the *t* plot model, whereas total pore volumes ( $V_{\text{total}}$ ) – the single point approach taking into account amounts of N<sub>2</sub> adsorbed at relative pressures  $p/p_0 \approx 0.99$ .

High-angle annular dark-field (HAADF) images, elemental mappings and EDX spectra were collected on a JEOL-2100F microscope in scanning transmission electron microscopy

(STEM) mode. In order to eliminate an influence of copper element from a grid, SiO grids were used in this work.

X-ray photoelectron spectroscopy (XPS) analyses were carried out in a system constructed by Prevac, equipped with a hemispherical analyzer (VG SCIENTA R3000) and a monochromatized aluminum source  $AlK\alpha$  ( $E = 1486.6$  eV). To compensate a charge on a surface of nonconductive samples, a low energy electron flood gun (FS40A-PS) was used. Binding energies in the measured spectra were corrected by referring to a position of Si 2p peak ( $E_b = 103.0$  eV). Deconvolution was done after fitting the Shirley background using a peak shape described by the mixed function of Gauss and Lorentz ( $GL = 30$ ). The spectra were processed using the CasaXPS software.

Temperature-programmed reduction ( $H_2$ -TPR) measurements were performed in a home-made equipment. An amount of 0.05 g of a sample was placed in a quartz microreactor in a flow of Ar/ $H_2$  mixture (95/5). The total flow rate of the reducing mixture was  $22$  mL  $min^{-1}$ . The  $H_2$ -TPR profiles were collected at a linear increase in temperature (heating rate of  $10$  °C $\cdot$ min $^{-1}$ ) within the range of 100-900 °C using a thermal conductivity detector placed at the reactor outlet directly after a cold trap ( $-40 \pm 3$  °C) used to remove produced water. The amount of hydrogen consumed during the reduction reaction was calculated based on calibration with CuO as a reference.

Acidic properties of samples were assessed by adsorption of pyridine (Py) followed by infrared spectroscopy (IR). The samples were pressed at  $\sim 1$  ton  $cm^{-2}$  into thin wafers of ca.  $10$  mg  $cm^{-2}$ . Prior to the pyridine adsorption/desorption experiments, the wafers were placed inside an infrared cell and activated under static conditions in  $O_2$  ( $1.6 \cdot 10^4$  Pa) at 450 °C for 3 h and outgassed at 300 °C ( $10^{-3}$  Pa) for 1 h. Subsequently, pyridine was introduced (133 Pa) into the cell at room temperature. The IR spectra were collected on a Bruker Vector 22 spectrometer (resolution  $2$   $cm^{-1}$ , 128 scans) after outgassing at 150 °C for 1 h. The resulting

spectra were obtained after subtraction of the spectrum recorded before pyridine adsorption. The quantification of acid sites was carried out as reported by Emeis [46].

### **2.3. Catalytic testing**

Catalytic combustion of toluene and benzene was conducted in a quartz microreactor with an inner diameter of 8.0 mm. A catalyst (0.1 g, particle size 160–315  $\mu\text{m}$ ) was inserted into the middle of reactor on a quartz wool plug. Before a catalytic run, the catalyst was degassed at 500 °C for 30 min in flowing air (100 mL·min<sup>-1</sup>). Then, the reactor was cooled to 200 °C and dosing aromatic hydrocarbon at concentration of 1000 ppm began. The organic substrate was introduced into the feed using a thermostated scrubber filled with liquid compounds kept at temperature ensuring its vapor pressure at the assumed level. The catalytic activity was studied at 200, 250, 275, 300, 325, 350, 400, 450 and 500 °C. The reactor was maintained at each temperature during three analyzes of reaction products (ca. 70 min), and then heated to a higher temperature at a heating ramp of 10 °C·min<sup>-1</sup>. The reaction products were analyzed using a Bruker 450 gas chromatograph equipped with two capillary columns (Porapak S and Chromosorb WAW-DMCS), two flame ionization detectors, a thermal conductivity detector and a methanizer.

In addition, stability tests in the toluene combustion were carried out maintaining identical experimental conditions with the only difference that after degassing the reactor was cooled to 300 °C. Then, at this temperature toluene dosing was turned on (optionally 5 vol% of water vapor was additionally introduced into the feed using a syringe pump), and the reaction products were analyzed periodically during the next 24 h.

### 3. Results and discussion

#### 3.1. Structural and textural properties of the Cu-Mn/BEA catalysts

BEA-supported catalysts containing different copper to manganese molar ratios for the total oxidation of VOCs were synthesized by the conventional wet impregnation method. Regardless of the amount of transition metal(s) introduced, the reflections attributed to the BEA structure (among them the most intense diffraction lines are centered at  $7.5^\circ$  (101),  $21.4^\circ$  (300),  $22.4^\circ$  (302),  $25.3^\circ$  (304) and  $27.1^\circ$  (006) [PDF 00-056-0467]) are identified in the XRD patterns of all calcined materials (Fig. 1) [47]. In addition to the above mentioned reflections, in the XRD patterns the features typical of metal oxide phases are found. For the samples lacking a second transition metal, i.e. Cu10SiBEA and Mn10SiBEA, the diffraction lines typical of the CuO or Mn<sub>2</sub>O<sub>3</sub> phases, respectively, are observed. For the sample containing 10 wt% of Cu, the (002) and (111) diffraction lines characteristic for the monoclinic structure of CuO nanoparticles appear at  $35.6^\circ$  and  $38.8^\circ$ , respectively [PDF 00-041-0254]. In turn, in the case of the Mn10SiBEA catalyst the peak at  $32.9^\circ$  is indexed as the (222) reflection of the cubic Mn<sub>2</sub>O<sub>3</sub> phase [PDF 00-041-1442]). Other reflections most likely exhibit too low intensity to be clearly detected in the recorded diffractograms, that may indicate a high degree of manganese oxide dispersion and its low crystallinity.

It should be assumed that, as in previously presented papers [48,49], for the mixed oxide systems with a Cu/Mn molar ratio  $< 0.5$  the Cu-doped Mn<sub>3</sub>O<sub>4</sub> phase with the tetragonal hausmannite structure is formed due to the Jahn–Teller distortion. Its high dispersion, as in the case of Mn<sub>2</sub>O<sub>3</sub> in the Mn10SiBEA sample, causes that no intense diffraction lines attributed to this phase are noticeable in the XRD pattern collected for Cu2Mn8SiBEA. After the introduction of higher amount of Cu, the distortion of spinel lattice disappears. Therefore, the two-component, Cu-rich catalysts (Cu4Mn6SiBEA, Cu5Mn5SiBEA, Cu6Mn4SiBEA, and Cu8Mn2SiBEA) show the reflections at ca.  $36.0^\circ$ ,  $57.8^\circ$  and  $63.5^\circ$  corresponding to the *hkl*

planes (311), (511) and (440), respectively, that indicate the formation of the spinel ( $\text{Cu}_x\text{Mn}_{3-x})_{1-\delta}\text{O}_4$  cubic phase [PDF 01-076-2296].

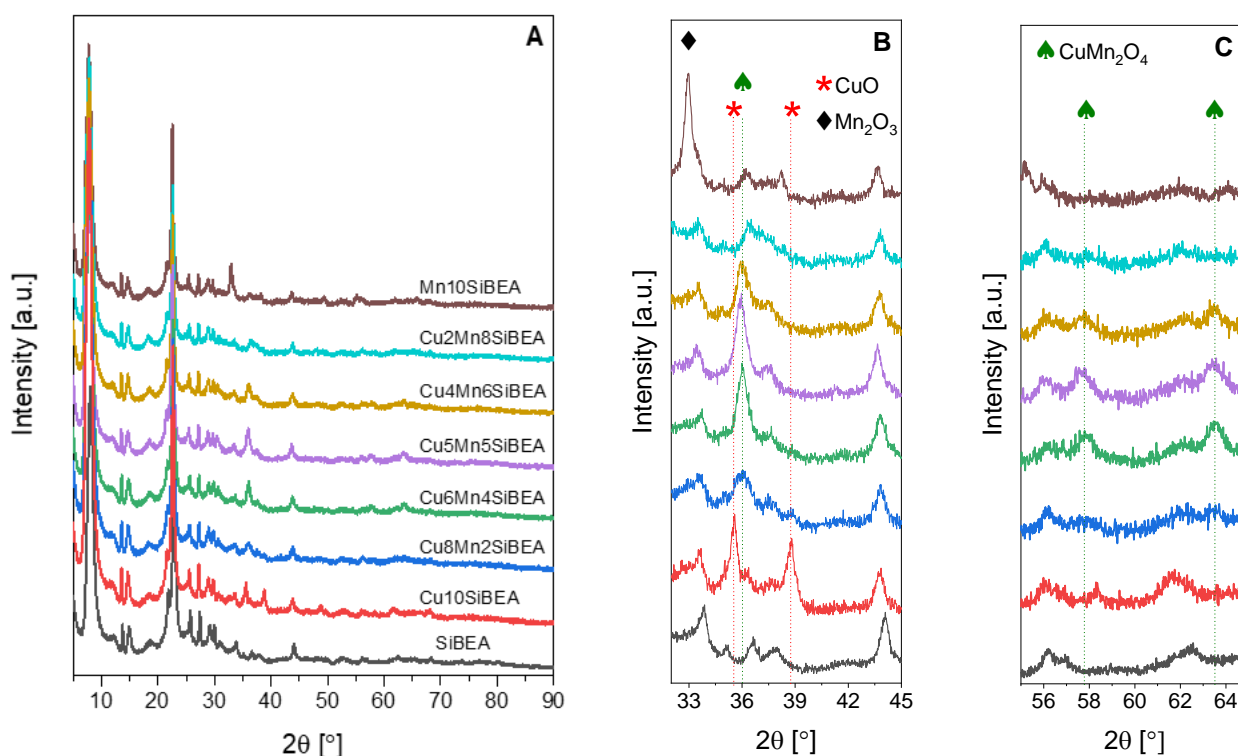


Figure 1. X-ray diffraction patterns of SiBEA before and after deposition of the Cu-Mn containing active phase (A) with the magnified  $2\theta$  range of  $32\text{-}45^\circ$  (B) and  $55\text{-}65^\circ$  (C).

Due to the very small size of the crystallites (estimated using the Scherrer equation based on the position of the (311) reflection) within the range from 2.7 nm ( $\text{Cu}_8\text{Mn}_2\text{SiBEA}$ ) to 8.7 nm ( $\text{Cu}_6\text{Mn}_4\text{SiBEA}$ ), it is difficult to precisely determine the lattice parameters. Nevertheless, it can be noticed that they differ slightly between the samples ( $a = b = c = 0.828 \pm 0.001$  nm), but no clear correlation between the calculated values and the relative content of Cu and Mn is found. These discrepancies are rather expected, because in the  $(\text{Cu}_x\text{Mn}_{3-x})_{1-\delta}\text{O}_4$  spinel structure the metal cations can be incorporated in different positions at various oxidation states (i.e.  $\text{Cu}^+$ ,  $\text{Cu}^{2+}$ ,  $\text{Mn}^{2+}$ ,  $\text{Mn}^{3+}$ ,  $\text{Mn}^{4+}$ ).

Table 1. Transition metal content, textural properties and concentration of acid sites for the studied BEA-based materials.

Sample	Mn content [wt %]	Cu content [wt %]	Cu/Mn molar ratio	Textural parameters					Lewis acidity
				$S_{\text{BET}}$ [m <sup>2</sup> /g]	$S_{\text{Langmuir}}$ [m <sup>2</sup> /g]	t-plot external surface area [m <sup>2</sup> /g]	$V_{\text{micro}}$ [cm <sup>3</sup> /g]	$V_{\text{total}}$ [cm <sup>3</sup> /g]	PyL ca. 1450 cm <sup>-1</sup> [μmol/g]
SiBEA	-	-	-	686	910	102	0.258	0.740	0.00
Cu10SiBEA	0.0	9.8	-	530	706	87	0.195	0.499	150.96
Cu8Mn2SiBEA	2.4	7.7	2.88	483	630	78	0.174	0.501	n.m.
Cu6Mn4SiBEA	3.5	6.1	1.56	477	634	77	0.176	0.446	n.m.
Cu5Mn5SiBEA	5.3	4.5	0.76	507	675	81	0.188	0.496	104.04
Cu4Mn6SiBEA	5.6	4.2	0.67	509	675	75	0.192	0.499	n.m.
Cu2Mn8SiBEA	8.7	1.9	0.20	499	663	75	0.188	0.502	n.m.
Mn10SiBEA	10.0	-	-	504	670	77	0.189	0.475	68.20

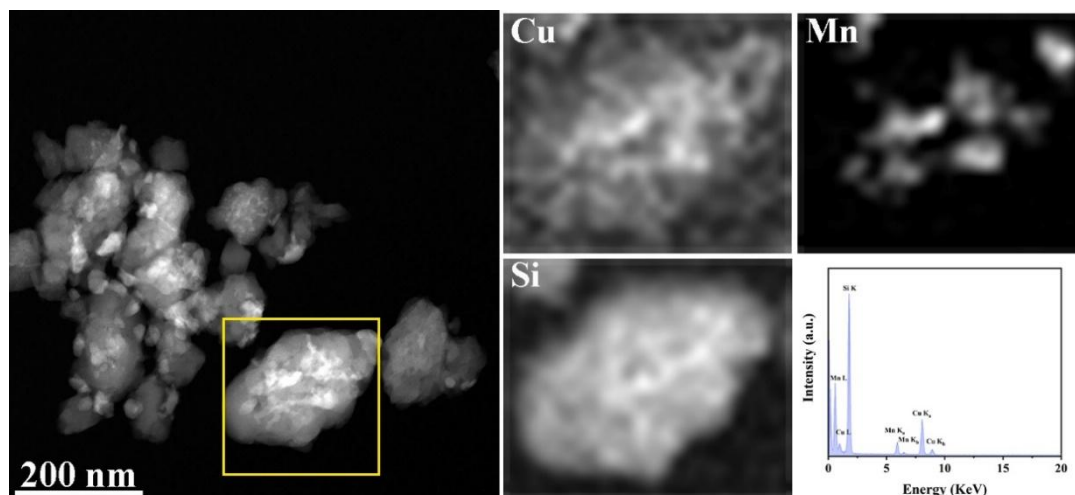


Figure 2. HAADF survey of  $\text{Cu}_2\text{Mn}_8\text{SiBEA}$ , corresponding elemental mappings and EDX spectrum for selected area.

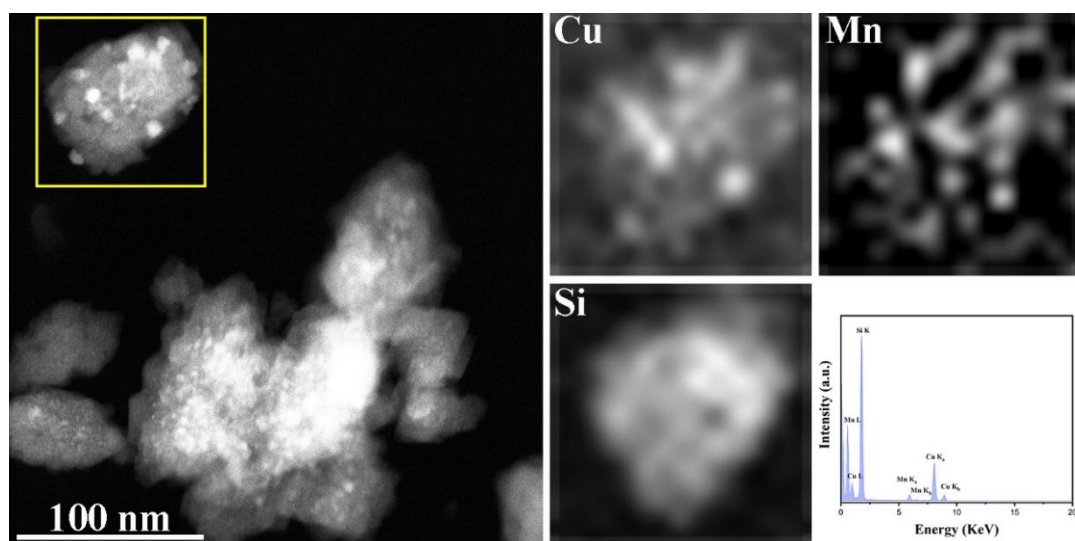


Figure 3. HAADF survey of  $\text{Cu}_8\text{Mn}_2\text{SiBEA}$ , corresponding elemental mappings and EDX spectrum for selected area.

Chemical composition of the tested materials was checked by XRF. The contents of Cu and Mn shown in Table 1 confirm the synthesis of the catalysts with metal loadings very close to the expected ones. The Cu/Mn molar ratios in the two-component samples increase in the range from 0.20 ( $\text{Cu}_2\text{Mn}_8\text{SiBEA}$ ) to 2.88 ( $\text{Cu}_8\text{Mn}_2\text{SiBEA}$ ). Furthermore, dispersion of main components in the BEA-based catalysts was examined by the STEM-EDX technique. The use

of HAADF detector results in a mass-thickness contrast. The yellow boxes, marked on the images taken for Cu<sub>2</sub>Mn<sub>8</sub>SiBEA and Cu<sub>8</sub>Mn<sub>2</sub>SiBEA (shown in Figure 2 and 3, respectively), denote the regions selected for the EDX analysis of Cu, Mn and Si. The observed strong Si signal is attributed to this element incorporated into the zeolite structure as well as the use of SiO grids. On the other hand, the EDX spectra show clear Cu and Mn signals, indicating high deposition of Cu and Mn species on the samples. Nevertheless, Cu has a more uniform distribution among the selected areas compared to Mn. It may suggest that some copper forms separate particles of the active phase.

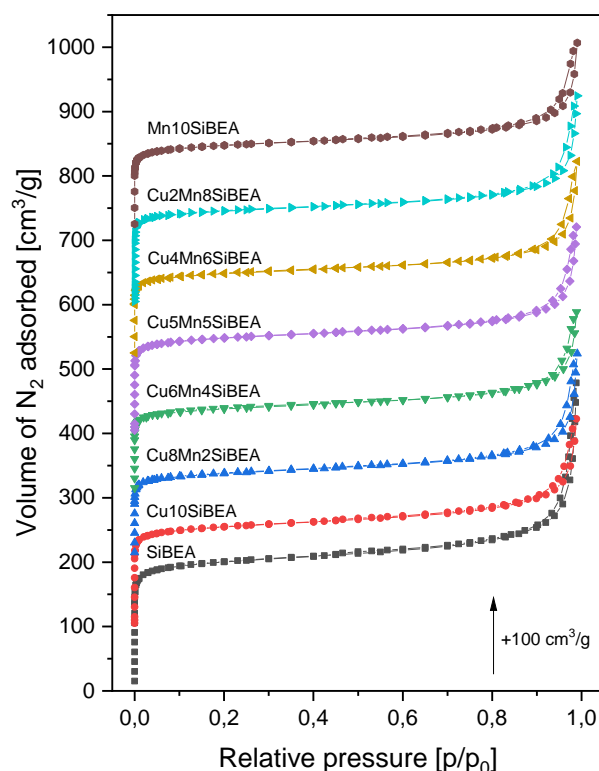


Figure 4. N<sub>2</sub> adsorption-desorption isotherms of SiBEA before and after deposition of the Cu-Mn containing active phase.

As determined by the N<sub>2</sub> adsorption measurements, the starting SiBEA material exhibits a type I isotherm (according to the IUPAC classification) characteristic for microporous materials (Fig. 4). The formally calculated S<sub>BET</sub> value for this support is 686 m<sup>2</sup>/g (S<sub>Langmuir</sub> = 910 m<sup>2</sup>/g) and the V<sub>total</sub> - 0.740 cm<sup>3</sup>/g (Table 1). It should be noted that only ca. 35% of the

$V_{\text{total}}$  is generated by micropores. The remaining pores are mainly large interparticle voids, whose presence is manifested by an increase in the amount of adsorbed nitrogen observed at the highest relative pressures ( $p/p_0 > 0.9$ ). The introduction of the transition metal-containing active phase results in a decrease in the  $S_{\text{BET}}$  and the  $S_{\text{Langmuir}}$  by 22-31 %. Simultaneously, the  $V_{\text{micro}}$  drops by 24-33% and the  $V_{\text{total}}$  by 32-40%. Therefore, it is clearly visible that the formed oxide crystallites partially block the pores of the support. However, they affect more significantly the macropores than the micropores, indicating a preferential location of the oxide crystallites in the interparticle spaces. Such a conclusion is rational due to the sizes of these crystallites significantly higher than the pore diameters in the SiBEA zeolite.

### 3.2. Surface acidity of the Cu-Mn/BEA catalysts

Acidity of the samples was studied by FT-IR after adsorption of pyridine (Fig. 5).

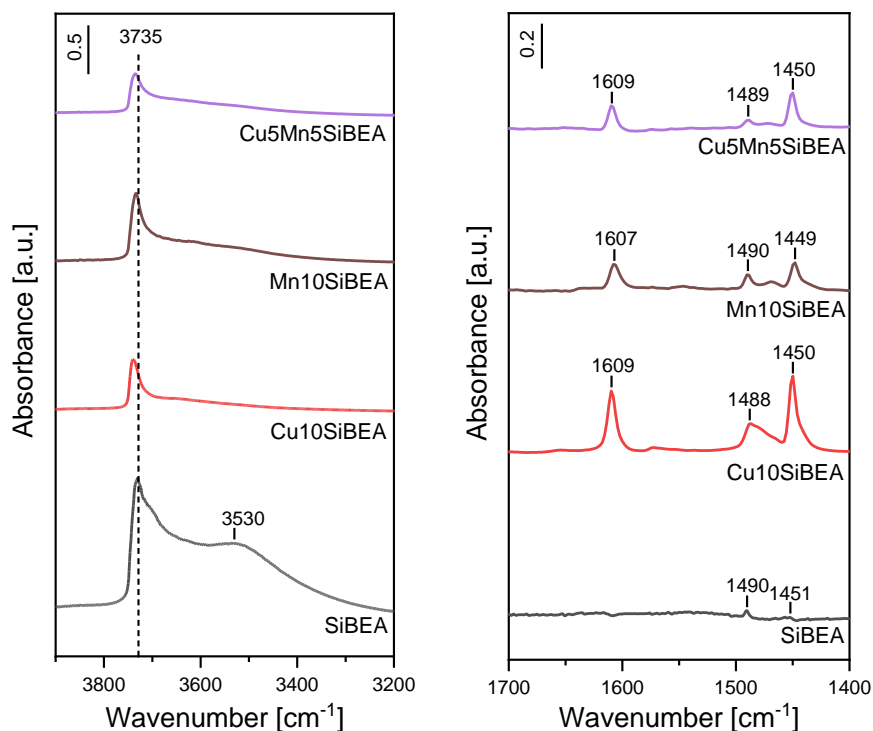


Figure 5. FT-IR spectra of the SiBEA-based materials pre-adsorbed with pyridine.

Typically, zeolites with low Si/Al ratios show relatively high concentration of acid sites formed in the zeolite structure because of the presence of  $\text{Al}^{3+}$  cations. The resulting negative

charge of the framework is counterbalanced by  $H^+$  ions attached to lattice oxygen atoms connecting adjacent silicon and aluminum atoms. Such protons play a role of Brønsted acid sites. The investigated SiBEA zeolite was initially subjected to the dealumination process, which in a consequence resulted in an efficient elimination of majority of  $H^+$  ions from the BEA structure. Therefore, in the FTIR spectrum of SiBEA the band at  $1545\text{ cm}^{-1}$ , typical of pyridine molecules interacting with the Brønsted acid sites, is not observed. The absence of this band is also noticeable for SiBEA modified with Cu and/or Mn. On the other hand, for the parent SiBEA zeolite the narrow intense band at  $3736\text{ cm}^{-1}$  related to isolated internal silanol groups and of the broad band at  $3530\text{ cm}^{-1}$  due to H-bonded SiOH groups are observed (Fig. 5). The latter band reveals the formation of vacant T-atom sites associated with silanol groups, in line with earlier data for SiBEA zeolites [50-52]. Upon impregnation of the SiBEA zeolite with the copper nitrate and manganese nitrate solutions as well as co-impregnation of both solutions the intensity of the silanol bands at  $3736$  and  $3520\text{ cm}^{-1}$  is reduced, particularly that at  $3520\text{ cm}^{-1}$  corresponding to the H-bonded SiOH groups (Fig. 5), suggesting that the silanol groups interact with the copper and manganese species [53-55]. The discussed deficiency of Brønsted acidity is compensated in the Cu- and/or Mn-doped samples by the presence of Lewis acid centers. Their relatively high surface concentration is manifested by three bands at  $1449\text{-}1451\text{ cm}^{-1}$ ,  $1488\text{-}1490\text{ cm}^{-1}$  and  $1607\text{-}1610\text{ cm}^{-1}$  [56]. A clear correlation between the type of doped metal and the number of the generated Lewis acid centers is found (Table 1). And so, for the unmodified SiBEA support the presence of Lewis acidity is negligible, while the highest numbers of such sites are observed for the Cu-rich materials. From this point of view, the doping with Mn encourages the appearance of a lower number of Lewis acid centers. It should be kept in mind that gaseous oxygen (being typical Lewis base) participating in the catalytic oxidation process can be easily adsorbed on the Lewis acid centers and converted to various reactive surface species, such as  $O^{2-}$ ,  $O_2^{2-}$  and  $O^-$  [57].

### 3.3. Coordination of transition metal active sites in the Cu-Mn/BEA catalysts

Coordination of transition metal species dispersed on the surface of BEA zeolite was examined by UV-vis-DR spectroscopy.

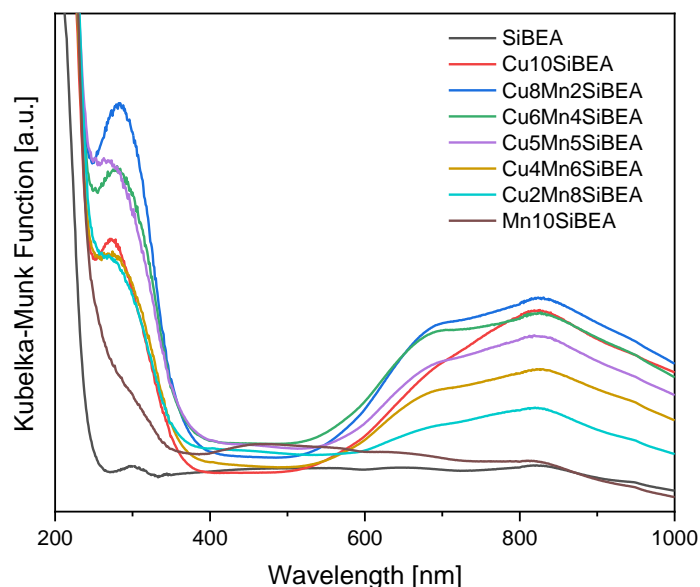


Figure 6. UV-vis-DR spectra of SiBEA before and after deposition of the Cu-Mn containing active phase.

In the spectra presented in Figure 6, features typical of the ligand-to-metal charge-transfer (CT) transitions between the surface  $O^{2-}$  and metal ions are observed at low wavelengths. The CT band is more distinct for the Cu-rich samples, where it appears around 280 nm with a shoulder at higher wavelengths due to the formation of  $Cu^{2+}-O^{2-}-Cu^{2+}$  clusters and highly dispersed CuO nanocrystallites. An increase in the Mn content leads to widening of this band as well as a loss of its intensity. Obviously, the Mn-containing species are not so highly ordered as copper-containing ones, which may be due to the presence of many low crystalline Mn oxide and hydroxide forms with varying degrees of dispersion. Similar conclusions can be drawn after analyzing the recorded UV-vis-DR spectra in the range of d-d transitions (above 600 nm). For the Mn10SiBEA material no intense band is found there, because the d-d transitions originated from  $Mn^{n+}$  occur below 500 nm. On the other hand, the

UV-vis-DR spectrum of Cu10SiBEA shows a wide band centered at 820 nm, which can be attributed to the  ${}^2E_g \rightarrow {}^2T_{2g}$  spin-allowed transitions of  $\text{Cu}^{2+}$  cations situated in the distorted octahedral symmetry of CuO [58]. For the samples with coexisting Mn, another band is distinguished at ca. 680 nm. Considering the appearance of  $(\text{Cu}_x\text{Mn}_{3-x})_{1-\delta}\text{O}_4$  spinel phase in these samples (confirmed by XRD), the presence of this band confirms the location of  $\text{Cu}^{2+}$  in the tetrahedral sites of this partly inverse spinel structure [59].

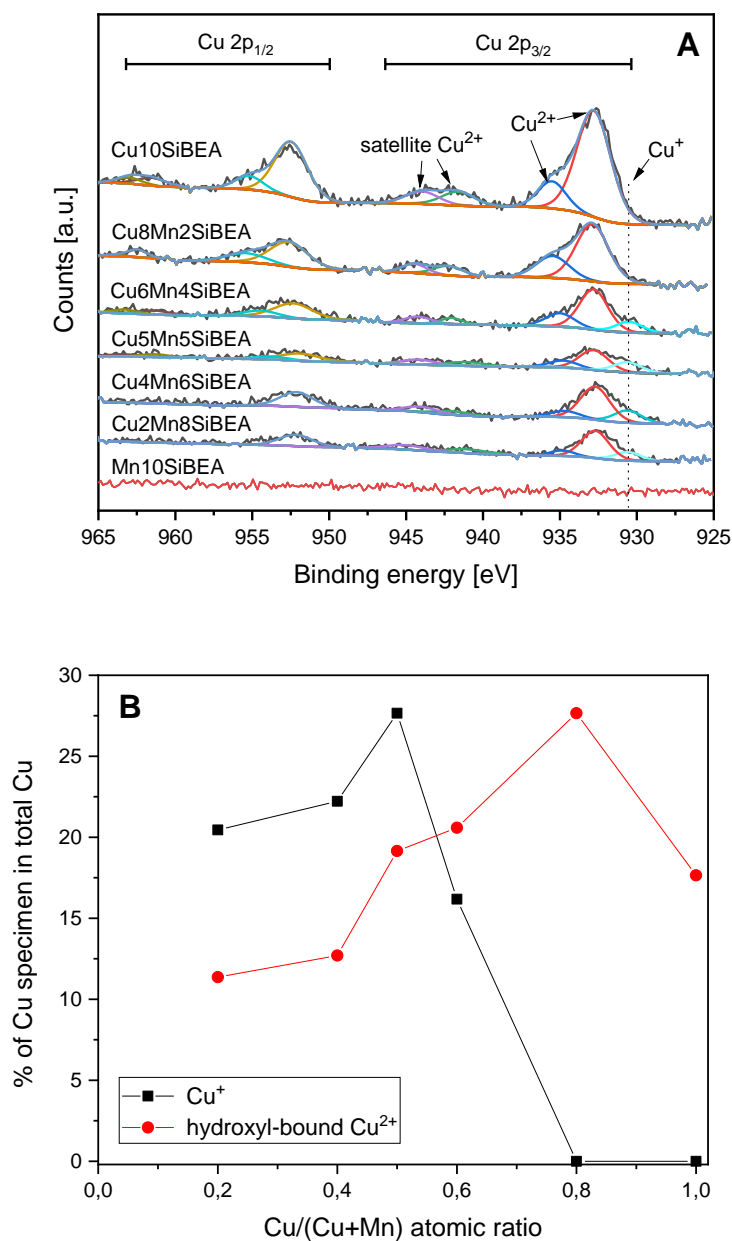


Figure 7. High-resolution XPS Cu 2p spectra (A) and distribution of various surface Cu forms determined by XPS (B).

XPS is another valuable tool providing insight into the surface composition of the studied samples. The measured survey spectra show the presence of peaks associated with photoemission from the core levels of all elements distributed in the structure (i.e., Si, O, Cu and Mn). Nevertheless, the content of transition metals (for all samples below 4.0 at%) indicates their successful deposition in the zeolite channels as well as interparticle voids without any enrichment on the external surface of grains.

The XPS O 1s spectra (not shown) are dominated by the presence of two components at  $532.2 \pm 0.2$  eV and  $533.1 \pm 0.2$  eV, which correspond to oxygen atoms in hydroxyls (and/or adsorbed oxygen-containing species) and water molecules, respectively. Apart from these forms of oxygen species, expected for the surface of BEA, very low peak at  $529.4 \pm 0.2$  eV, attributed to  $O^{2-}$ , appears in the XPS O 1s spectra of the Cu- and Mn-doped catalysts. It should be emphasized, however, that the content of the latter form of oxygen does not exceed 3% of the total number of oxygen atoms detected by XPS.

Unfortunately, multiplet splitting observed for the Mn 2p peak excludes the reliable discussion of Mn oxidation states. The Mn 3s region, often used for this purpose [60], is not also helpful in resolving this issue due to the low concentration of Mn in the tested samples - the intensity of the measured Mn 3s signals is hardly distinguished from the background level. Therefore, the most important information about the state of the surface can be obtained from the analysis of XPS Cu 2p spectra consisting two main regions (Cu 2p<sub>3/2</sub> and Cu 2p<sub>1/2</sub>) due to spin-orbit coupling (Fig. 7A). In the Cu 2p<sub>3/2</sub> region of the Cu<sub>10</sub>SiBEA and Cu<sub>8</sub>Mn<sub>2</sub>SiBEA catalysts, two peaks at  $932.8 \pm 0.1$  eV and  $935.0 \pm 0.3$  eV (attributed to Cu<sup>2+</sup> ions surrounded by O<sup>2-</sup> and OH<sup>-</sup> ions, respectively) with very intense satellite features at ~942 eV and 944 eV are found [58]. An increase in the Mn content results in a gradual decrease in the number of superficial hydroxyl-bound Cu<sup>2+</sup> species (Fig. 7B) and an appearance of additional peak at 930.5 eV corresponding to Cu<sup>+</sup> [61]. The presence of Cu<sup>0</sup> was excluded based on the analysis

of the  $L_3M_{4.5}M_{4.5}$  Auger spectra [62]. The described finding confirms that both  $Cu^{2+}$  and  $Cu^+$  ions co-exist in the created  $(Cu_xMn_{3-x})_{1-\delta}O_4$  spinel phase. The latter ones appear together with  $Mn^{4+}$  as a result of redox equilibrium  $Cu^{2+} + Mn^{3+} = Cu^+ + Mn^{4+}$ , which was previously discussed by Papavasiliou et al. [63]. The highest content of  $Cu^+$  is reached for the Cu5Mn5SiBEA sample with equimolar participation of Cu and Mn in the active phase (Fig. 7B).

### 3.4. Reducibility of the Cu-Mn/BEA catalysts

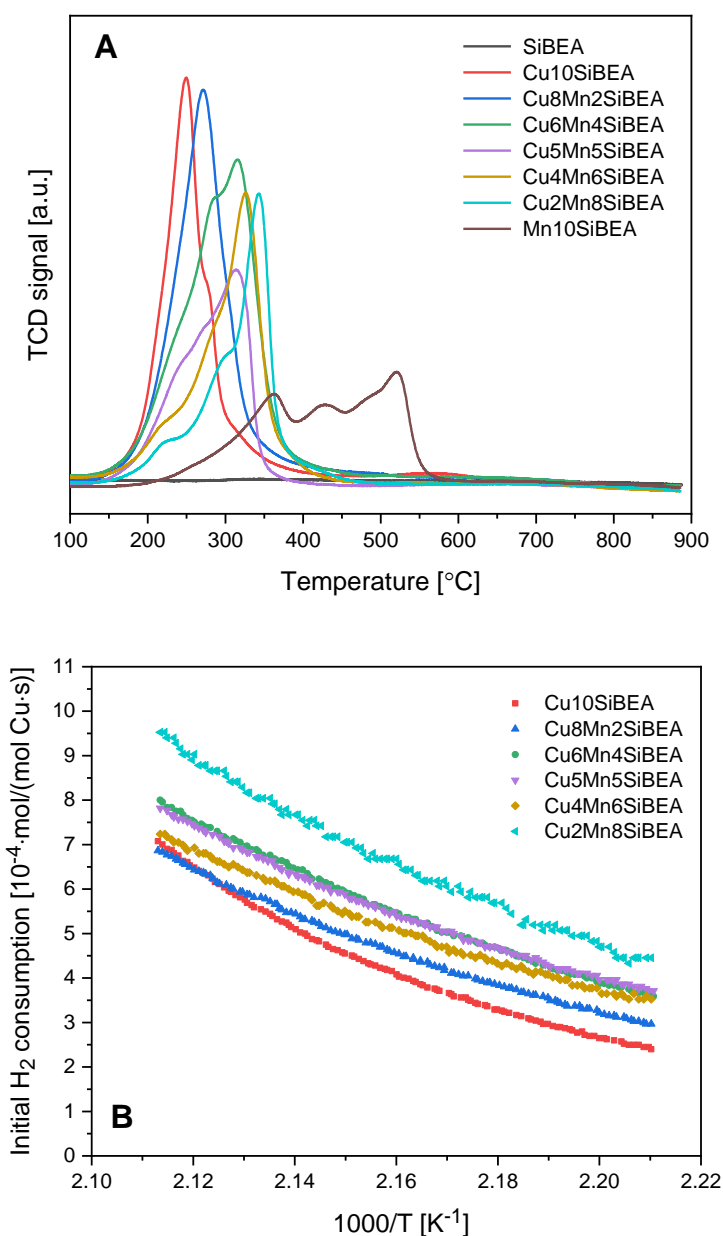


Figure 8. H<sub>2</sub>-TPR profiles (A) and initial H<sub>2</sub> consumption rate as a function of inverse temperature (B) for SiBEA before and after deposition of the Cu-Mn containing active phase.

In Figure 8A the H<sub>2</sub>-TPR profiles recorded for the SiBEA-supported catalysts are shown. Evidently, the samples containing only one type of transition metal (Cu or Mn) differ significantly in their reducibility. The reduction of Cu10SiBEA begins at a temperature as low as 130 °C and reaches its maximum rate at ca. 250 °C. This process is so fast that usually postulated two stages of CuO reduction ( $\text{Cu}^{2+} \rightarrow \text{Cu}^+$  followed by  $\text{Cu}^+ \rightarrow \text{Cu}^0$  [36,64]) overlap to give one reduction peak. Nevertheless, on its high-temperature side at about 280 °C, a shoulder appears, which indicates the presence of harder reducible Cu forms. The latter reduction effect most likely comes from the  $\text{Cu}^{n+}$  ions and  $\text{CuO}_x$  clusters present in the non-framework positions in the channels and on the surface of zeolite. These fine moieties are stabilized by interactions with the negatively charged zeolite framework. On the other hand, the reduction profile of the Mn10SiBEA sample is much more complex. Generally, the reduction of manganese phases requires definitely higher temperatures than for the copper-containing species and starts at ca. 180 °C. Two maxima at higher temperatures (425 °C and 520 °C) are attributed to the two-stage reduction of  $\text{Mn}_2\text{O}_3$  ( $\text{Mn}_2\text{O}_3 \rightarrow \text{Mn}_3\text{O}_4$  followed by  $\text{Mn}_3\text{O}_4 \rightarrow \text{MnO}$ ), as previously observed by Yang et al. [65]. In turn, the reduction peak at 360 °C shows that much easier reducible, surficial Mn specimens are also present on the Mn10SiBEA surface.

In the case of the preparations containing Cu and Mn simultaneously, the reduction starts at a temperature similar to that found for Cu10SiBEA. However, the main reduction peaks gradually widen and move to higher temperatures. It can be noticed that the amount of easily reducible Cu species decreases with the increasing total Cu loading. Their presence is manifested by the shoulder at approx. 230 °C observed mainly for the samples with the low Cu loadings. This effect is supported by analyzing the initial rate of H<sub>2</sub> consumption versus

inverse temperature (Figure 8B), which is the highest for Cu<sub>2</sub>Mn<sub>8</sub>SiBEA. Nevertheless, it can be concluded that the presence of manganese strongly stabilizes the oxidation state of copper ions (Cu<sup>2+</sup> and Cu<sup>+</sup>), which occupy the positions in the Mn<sub>3</sub>O<sub>4</sub> and/or Cu<sub>x</sub>Mn<sub>3-x</sub>)<sub>1-δ</sub>O<sub>4</sub> structures as confirmed by XRD and XPS studies. On the other hand, the reduction of Mn<sup>n+</sup> ions becomes noticeably easier compared to that of Mn<sub>2</sub>O<sub>3</sub> dominating in the Mn<sub>10</sub>SiBEA catalyst. Suffice it to say that for all copper-manganese samples the reduction process finishes essentially below 450 °C. The analogous effect promoting the reduction of Mn<sup>n+</sup> ions in the environment of Cu<sup>n+</sup> ions coexisting in one spinel phase was previously described by other researchers [25,63]. This mutual interaction of Mn<sup>n+</sup> and Cu<sup>n+</sup> ions changing the reduction mechanism can also be important for catalytic activity.

### **3.5. Catalytic activity of the Cu-Mn/BEA catalysts in VOCs combustion**

The developed SiBEA-based materials were tested as catalysts in the total oxidation of toluene, representing a wide group of aromatic VOCs. Figure 9A shows the toluene conversions as a function of reaction temperature. After the introduction of transition metal (Cu and/or Mn), the catalytic activity of SiBEA zeolite increases drastically. In the case of these catalysts, the toluene conversion is observed already at 250 °C, which is in strong contrast to the parent SiBEA (showing low activity starting from 400 °C). This catalytic parameter increases with raising the reaction temperature. An influence of the type and content of the transition metal on the toluene conversion is clearly visible. At lower temperatures (250 and 275 °C) it correlates with the Cu content - the higher Cu loading, the higher toluene conversion (but not higher than 11%). However, an interesting effect is noted at 300 °C, where the catalysts are grouped into those containing a single transition metal and others containing Cu and Mn simultaneously. Double promotion has a clear beneficial effect on the catalytic activity in the toluene combustion. In a narrow temperature window (up to

350 °C), complete conversion of the aromatic substrate is achieved over all transition metal-loaded catalysts.

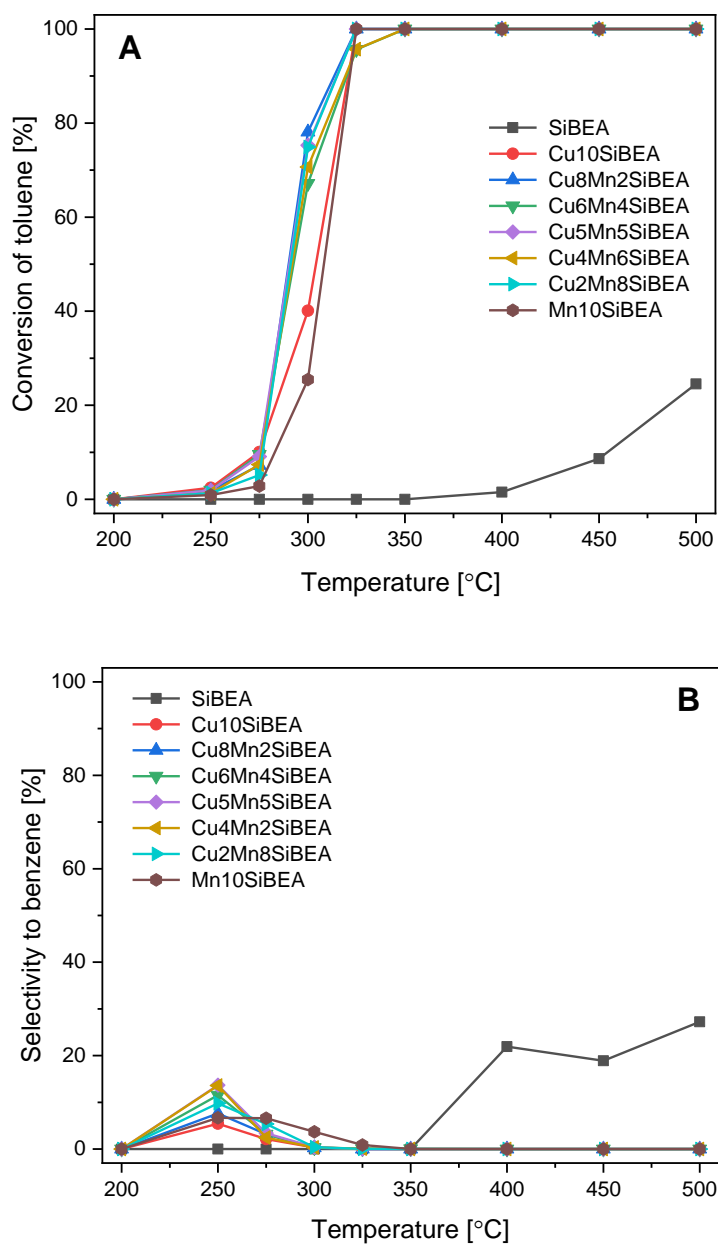


Figure 9. Catalytic performance of SiBEA before and after deposition of the Cu-Mn containing active phase in the toluene combustion: (A) conversion of toluene and (B) selectivity to benzene vs. reaction temperature.

The positive effect of mixing  $\text{Mn}^{3+}$  and  $\text{Cu}^{2+}$  cations in one oxide structure deposited on SiBEA is related to the possible electron migration between both metal sites. High

electronegativity of copper promotes the electron transfer from manganese, and the redox cycle of  $\text{Cu}^{2+}/\text{Cu}^+$  activating oxygen appears [66]. The formed oxygen vacancies, which facilitate adsorption of oxygen species, remain stable on the surface of active phase above 275 °C [67]. Generally, manganese oxides show tendency to the formation of surface defects, which can be additionally induced by chemical treatment (e.g., acid leaching [65]). Such vacancies can adsorb and activate gaseous oxygen, and subsequently improve mobility of formed surficial oxygen species. Most importantly, the adsorbed oxygen species are more reactive in the toluene combustion and easier to be replenished compared to lattice oxygen [35]. The involvement of lattice oxygen is very often considered in the total oxidation of VOCs in the so-called Mars van-Krevelen mechanism [40,68]. According to this mechanism, which is also assumed for the catalysts studied in this work, in the first step toluene molecules react with oxygen species built into the structure of the active phase surface. During the combustion reaction,  $\text{CO}_2$  and  $\text{H}_2\text{O}$  molecules as well as reduced active sites are produced. In the second step, the reduced active sites react with  $\text{O}_2$  molecules present in the gas phase reactivating the catalyst. For such a mechanism to be valid, a transition metal oxide phase must not interact too strongly with a support. This arrangement is obtained when using dealuminated BEA zeolite.

The presence of Lewis acid sites in the Cu-rich samples additionally promotes the appearance of reactive forms of chemisorbed oxygen, which are more strongly stabilized under reducing conditions in the Cu-Mn/SiBEA samples compared to Cu/SiBEA, as confirmed by the results of  $\text{H}_2$ -TPR studies. Hence, the catalysts based on mixed Cu-Mn systems show excellent catalytic properties at higher reaction temperatures (> 275 °C), in which the surface of one component Cu10SiBEA is deeply reduced and its regeneration with molecular oxygen is hindered. The presence of two kinds of Jahn-Teller ions ( $\text{Mn}^{3+}$  and  $\text{Cu}^{2+}$ ) in the spinel structure additionally facilitates solid state charge transfer redox system ( $\text{Cu}^{2+} +$

$\text{Mn}^{3+} = \text{Cu}^+ + \text{Mn}^{4+}$ ) [43]. Therefore, in the temperature window of catalytic performance up to 300 °C the valency of the surface Cu is almost completely preserved, as confirmed by the XPS measurements carried out for the Cu<sub>6</sub>Mn<sub>4</sub>SiBEA catalyst after the toluene combustion process interrupted at 275 or 300 °C (Fig. 10). In both spent samples the intense component at 930.5 eV assigned to Cu<sup>+</sup> is observed. On the other hand, an increase in the participation of Cu<sup>2+</sup>-OH<sup>-</sup> species is found, especially after the reaction at 275 °C. Thus, surface hydroxylation occurs under the moisture-rich reaction conditions. Furthermore, slightly higher contents of surface carbon appear in these samples after the catalytic run (Fig. 10). The fresh Cu<sub>6</sub>Mn<sub>4</sub>SiBEA catalyst contains 0.9 at.% of C, whereas after the reaction this amount increases to 3.7 at.% (the process stopped at 275 °C) or 2.8 at.% (the process stopped at 300 °C). This is not surprising, since the oxidation of toluene most likely undergoes through several steps: (i) adsorption of an aromatic hydrocarbon molecule onto an active site with the formation of benzoyl species by abstraction of H from a methyl group, (ii) transformation of benzoyl into intermediates, such as benzyl alcohol, benzaldehyde, and benzoate species, (iii) reaction with oxygen species to produce intermediates without aromatic ring, such as maleic anhydride and carboxylate species, and finally (iv) the deepest oxidation to CO<sub>2</sub> and H<sub>2</sub>O. Some of these intermediates may remain on the surface, creating a relatively small amount of carbon deposit. This reaction mechanism was confirmed by DRIFT studies carried out by various authors for Cu-Mn-O catalysts [69-71].

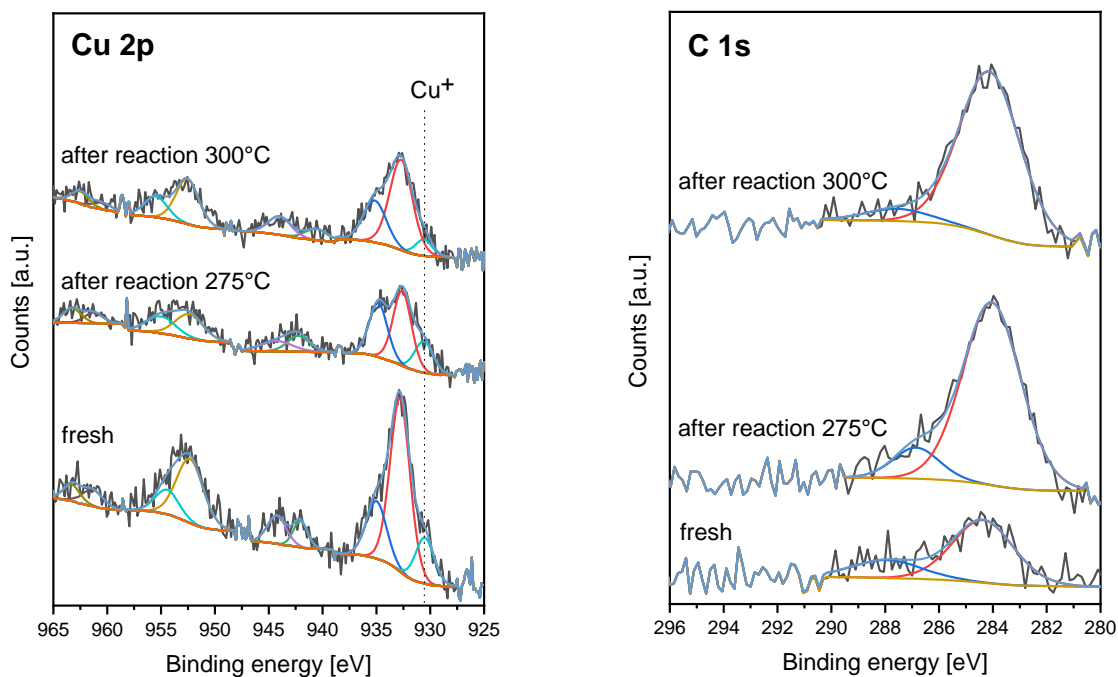


Figure 10. Comparison of high-resolution XPS Cu 2p and C 1s spectra for fresh and spent Cu<sub>6</sub>Mn<sub>4</sub>SiBEA. The samples after the reaction of toluene combustion stopped at 275 or 300 °C were immediately transferred to the XPS spectrometer.

If we look at selectivity of the tested Cu-Mn/SiBEA catalysts, we find that next to the expected products of complete oxidation of toluene (CO<sub>2</sub> and H<sub>2</sub>O), the formation of minor amounts of benzene is observed, which occurs especially at low temperatures (Fig. 9B). CO and other by-products formation is negligible. The appearance of benzene as a main by-product is reasonable due to the formation of benzoyl species (postulated as the former step of the toluene combustion mechanism) that may crack. At low temperatures, when the rate of consecutive steps is not high enough, probability of their decomposition is relatively high. Therefore, for all Cu-loaded SiBEA catalysts the presence of benzene among products is observed only below 300 °C (for less active Mn<sub>10</sub>SiBEA and SiBEA benzene is produced also at higher temperatures). The selectivity to benzene is lower, the catalyst is more active in the toluene combustion. In addition, the developed Cu-loaded SiBEA catalysts are also active

in the combustion of benzene, and therefore  $C_6H_6$  released as a result of the decomposition of benzoyl groups may be burned after re-adsorption in a further part of the catalytic bed.

To recognize the catalytic activity of the studied materials in the total oxidation of benzene, we performed tests for this reaction under analogous conditions as in the case of the toluene combustion. The obtained results in the form of benzene conversion for three selected catalysts are shown in Figure 11. A correlation of catalytic activity with the copper content is found within the whole operating temperature window. The reaction starts at ca. 250 °C and accelerates with increasing temperature reaching 100% conversion around 450 °C. Thus, it can be concluded that benzene molecules are more difficult to oxidize over the tested catalysts compared to toluene molecules. This effect is quite reasonable due to different reaction mechanisms. It is generally believed that the presence of a methyl group in a toluene molecule facilitates oxidation of an aromatic ring compared to a benzene molecule, in which an aromatic ring has to be dissociated directly [72].

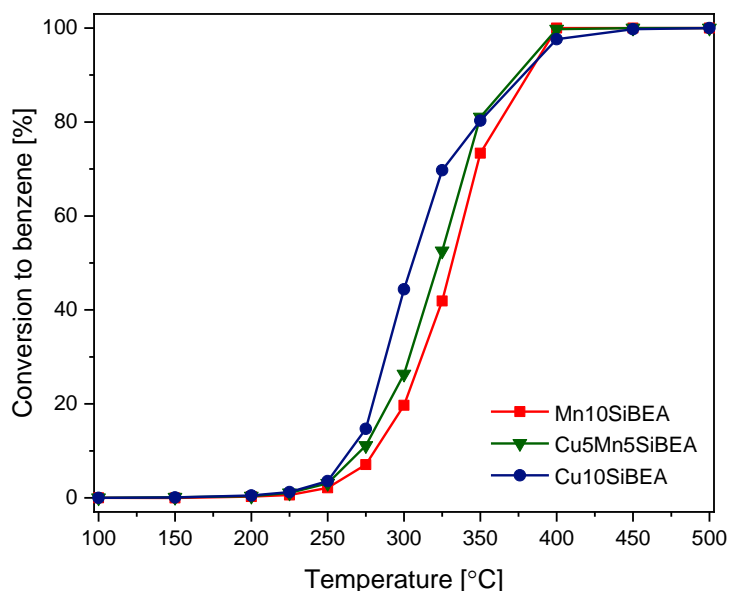


Figure 11. Conversion of benzene over Cu10SiBEA, Cu5Mn5SiBEA and Mn10SiBEA vs. reaction temperature.

Finally, we studied stability of the SiBEA-supported catalysts in the toluene combustion performed at 300°C. In Figure 12 changes in the toluene conversion during 24 h time-on-stream are compared for two chosen samples – Cu5Mn5SiBEA and Cu10SiBEA.

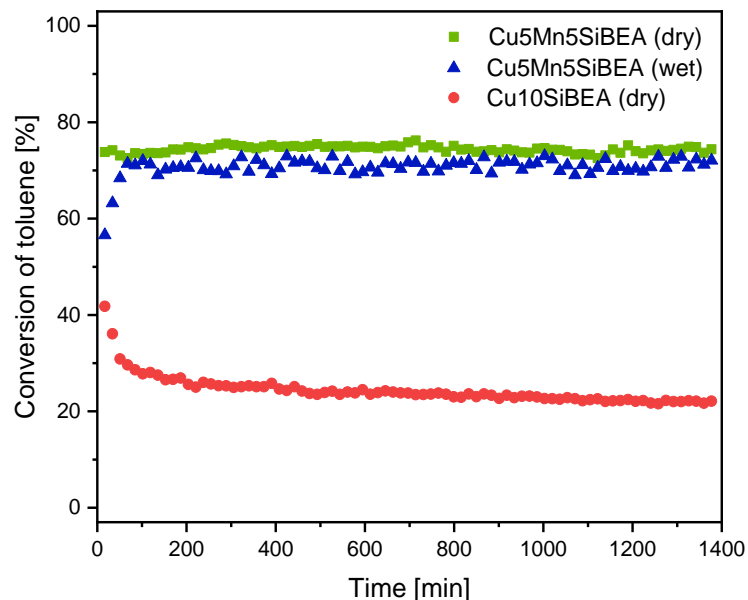


Figure 12. Stability tests in toluene combustion over Cu5Mn5SiBEA and Cu10SiBEA at 300°C under dry or wet atmosphere.

The great difference in activity of both materials at this moderate temperature is confirmed. However, one can find another feature distinguishing the catalysts containing only Cu from those additionally loaded with Mn. The Cu5Mn5SiBEA sample remains stable throughout the whole test, maintaining conversion of  $74.4 \pm 1.8\%$ . In turn, the Cu10SiBEA sample clearly loses its catalytic activity. During the first hour of the test, the conversion drops from 41.8% to 29.7%, and then it declines slowly reaching finally the level of  $22.0 \pm 0.4\%$ . Therefore, it can be concluded that promoting Cu-loaded SiBEA by introducing Mn significantly stabilizes the catalyst during its operation in the combustion of VOCs. The catalytic performance of Cu5Mn5SiBEA is high even in the presence of water vapor as confirmed by the results from the wet atmosphere test (5 vol% of moisture). In the initial period of 1 h the activity is admittedly lower than that observed during the dry atmosphere

test, but it quickly reaches a stable level just slightly lower (by about 3%) than that achieved in the environment without a significant excess of water vapor.

#### **4. Conclusion**

The developed modification method allows obtaining high dispersion of Cu and/or Mn oxide phases on a BEA zeolite support. By changing the Cu/Mn ratio in the mother solution, materials containing pure CuO, pure Mn<sub>2</sub>O<sub>3</sub> or mixed oxide systems, mainly of the (Cu<sub>x</sub>Mn<sub>3-x</sub>)<sub>1-δ</sub>O<sub>4</sub> spinel structure, were obtained. The introduction of the transition metal oxide particles into the BEA porous structure resulted in only slight decrease in texture parameters (specific surface area, volume of micropores, total pore volume) of the support. The observed changes in porosity in combination with the average size of the formed oxide phase particles evidently suggest the location of the active phase nanocrystallites in interparticle voids of BEA. The parent BEA zeolite was initially dealuminated, therefore the support used for modification was essentially free of acid sites. Nevertheless, the introduction of the transition metal oxide phases led to the appearance of Lewis acid centers, the concentration of which increased with raising Cu content. During the thermal treatment, Cu<sup>2+</sup> and Mn<sup>3+</sup> cations exhibiting the Jahn Teller effect were partially transformed into more stable Cu<sup>+</sup> and Mn<sup>4+</sup> ions. Their presence guaranteed stabilization of the system under reducing conditions, which, in combination with the presence of numerous surface vacancies, resulted in the high catalytic activity and stability of the developed catalysts in the total oxidation of toluene.

#### **Acknowledgements**

A.R. would like to thank for the financial support obtained under the French Government Scholarship program. The research was partially carried out with the equipment purchased thanks to the financial support of the European Regional Development Fund in the framework

of the Polish Innovation Economy Operational Program (contract no. POIG.02.01.00-12-023/08).

## References

- [1] Z. Zhang, Z. Jiang, W. Shangguan, Low-temperature catalysis for VOCs removal in technology and application: A state-of-the-art review, *Catalysis Today* 264 (2016) 270-278, <https://doi.org/10.1016/j.cattod.2015.10.040>.
- [2] P. Kuśtrowski, A. Rokicińska, T. Kondratowicz, Abatement of Volatile Organic Compounds Emission as a Target for Various Human Activities Including Energy Production, *Advances in Inorganic Chemistry* 72 (2018) 385-419, <https://doi.org/10.1016/bs.adioch.2018.05.004>.
- [3] L.F. Liotta, Catalytic oxidation of volatile organic compounds on supported noble metals, *Applied Catalysis B: Environmental* 100 (2010) 403-412, <https://doi.org/10.1016/j.apcatb.2010.08.023>.
- [4] M. Piumetti, D. Fino, N. Russo, Mesoporous manganese oxides prepared by solution combustion synthesis as catalysts for the total oxidation of VOCs, *Applied Catalysis B: Environmental* 163 (2015) 277-287, <https://doi.org/10.1016/j.apcatb.2014.08.012>.
- [5] P. Li, H. He, G. Wei, X. Liang, F. Qi, F. Tan, W. Tan, J. Zhu, R. Zhu, Effect of Mn substitution on the promoted formaldehyde oxidation over spinel ferrite: Catalyst characterization, performance and reaction mechanism, *Applied Catalysis B: Environmental* 182 (2016) 476-484, <https://doi.org/10.1016/j.apcatb.2015.09.055>.
- [6] S. Boycheva, D. Zgureva, M. Václavíková, Y. Kalvachev, H. Lazarova, M. Popova, Studies on non-modified and copper-modified coal ash zeolites as heterogeneous catalysts for VOCs oxidation, *Journal of Hazardous Materials* 361 (2019) 374-382, <https://doi.org/10.1016/j.jhazmat.2018.07.020>.

- [7] P. Natkański, A. Rokicińska, A. Wach, M. Drozdek, B. Dudek, L. Lityńska-Dobrzyńska, P. Kuśtrowski, Physicochemical properties of hydrogel template synthesized copper(II) oxide-modified clay influencing its catalytic activity in toluene combustion, *RSC Advances* 6 (2016) 100373-100382, <https://doi.org/10.1039/C6RA16278A>
- [8] Y. Shu, Y. Xu, H. Huang, J. Ji, S. Liang, M. Wu, D.Y.C. Leung, Catalytic oxidation of VOCs over Mn/TiO<sub>2</sub>/activated carbon under 185 nm VUV irradiation, *Chemosphere* 208 (2018) 550-558, <https://doi.org/10.1016/j.chemosphere.2018.06.011>.
- [9] X. Zhang, H. Zhao, Z. Song, J. Zhao, Z. Ma, M. Zhao, Y. Xing, P. Zhang, N. Tsubaki, Influence of hydrothermal synthesis temperature on the redox and oxygen mobility properties of manganese oxides in the catalytic oxidation of toluene, *Transition Metal Chemistry* 44 (2019) 663–670, <https://doi.org/10.1007/s11243-019-00331-5>.
- [10] S. Somekawa, H. Watanabe, Y. Oaki, H. Imai, VOC decomposition over a wide range of temperatures using thermally stable Cr<sup>6+</sup> sites in a porous silica matrix, *Catalysis Communications* 72 (2015) 161-164, <https://doi.org/10.1016/j.catcom.2015.09.019>.
- [11] E.J. Park, J.H. Lee, K.D. Kim, D.H. Kim, M.G. Jeong, Y.D. Kim, Toluene oxidation catalyzed by NiO/SiO<sub>2</sub> and NiO/TiO<sub>2</sub>/SiO<sub>2</sub>: Towards development of humidity-resistant catalysts, *Catalysis Today* 260 (2016) 100-106, <https://doi.org/10.1016/j.cattod.2015.03.038>.
- [12] M.G. Jeong, E.J. Park, B. Jeong, D.H. Kim, Y.D. Kim, Toluene combustion over NiO nanoparticles on mesoporous SiO<sub>2</sub> prepared by atomic layer deposition, *Chemical Engineering Journal* 237 (2014) 62-69, <https://doi.org/10.1016/j.cej.2013.09.100>.
- [13] J. Jacquemin, S. Siffert, J.F. Lamonier, E. Zhilinskaya, A. Aboukaïs, Catalytic properties of beta zeolite exchanged with Pd and Fe for toluene total oxidation, *Studies in Surface Science and Catalysis* 142 (2002) 699-706, [https://doi.org/10.1016/S0167-2991\(02\)80091-X](https://doi.org/10.1016/S0167-2991(02)80091-X).

- [14] R. Xie, G. Liu, D. Liu, S. Liang, D. Lei, H. Dong, H. Huang, D.Y.C. Leung, Wet scrubber coupled with heterogeneous UV/Fenton for enhanced VOCs oxidation over Fe/ZSM-5 catalyst, *Chemosphere* 227 (2019) 401-408, <https://doi.org/10.1016/j.chemosphere.2019.03.160>.
- [15] G. Li, C. Zhang, Z. Wang, H. Huang, H. Peng, X. Li, Fabrication of mesoporous  $\text{Co}_3\text{O}_4$  oxides by acid treatment and their catalytic performances for toluene oxidation, *Applied Catalysis A: General* 550 (2018) 67-76, <https://doi.org/10.1016/j.apcata.2017.11.003>.
- [16] A. Rokicińska, P. Natkański, B. Dudek, M. Drozdek, L. Lityńska-Dobrzyńska, P. Kuśtrowski,  $\text{Co}_3\text{O}_4$ -pillared montmorillonite catalysts synthesized by hydrogel-assisted route for total oxidation of toluene, *Applied Catalysis B: Environmental* 195 (2016) 59-68, <https://doi.org/10.1016/j.apcatb.2016.05.008>.
- [17] Z. Tian, N. Bahlawane, F. Qi, K. Kohse-Höinghaus, Catalytic oxidation of hydrocarbons over  $\text{Co}_3\text{O}_4$  catalyst prepared by CVD, *Catalysis Communications* 11 (2009) 118-122, <https://doi.org/10.1016/j.catcom.2009.09.008>.
- [18] S. Todorova, G. Kadinov, K. Tenchev, Y. Kalvachev, V. Kostov-Kytin, Particle size and support effects on the complete benzene oxidation by Co and Co-Pt catalysts, *Journal of Materials Science* 42 (2007) 3315–3320, <https://doi.org/10.1007/s10853-006-0894-x>.
- [19] X. Hu, Z. Zhang, Y. Zhang, L. Sun, H. Tian, X. Yang, Synthesis of a Highly Active and Stable Pt/ $\text{Co}_3\text{O}_4$  Catalyst and Its Application for the Catalytic Combustion of Toluene, *European Journal of Inorganic Chemistry* 2019 (2019) 2933-2939, <https://doi.org/10.1002/ejic.201900372>.
- [20] S. Todorova, G. Kadinov, K. Tenchev, A. Caballero, J.P. Holgado, R. Pereñíguez,  $\text{Co}_3\text{O}_4 + \text{CeO}_2/\text{SiO}_2$  Catalysts for n-Hexane and CO Oxidation, *Catalysis Letters* 129 (2009) 149–155, <https://doi.org/10.1007/s10562-008-9805-x>.

- [21] X. Zhang, J. Zhao, Z. Song, H. Zhao, W. Liu, Z. Ma, M. Zhao, H. Du, Cooperative Effect of the Ce–Co–O<sub>x</sub> for the Catalytic Oxidation of Toluene, *Chemistry Select* 4 (2019) 8902-8909, <https://doi.org/10.1002/slct.201902258>.
- [22] Y. Wang, H. Arandiyana, Y. Liu, Y. Liang, Y. Peng, S. Bartlett, H. Dai, S. Rostamnia, J. Li, Template-free Scalable Synthesis of Flower-like Co<sub>3-x</sub>Mn<sub>x</sub>O<sub>4</sub> Spinel Catalysts for Toluene Oxidation, *ChemCatChem* 10 (2018) 3429–3434, <https://doi.org/10.1002/cctc.201800598>.
- [23] W. Tang, X. Wu, S. Li, W. Li, Y. Chen, Porous Mn–Co mixed oxide nanorod as a novel catalyst with enhanced catalytic activity for removal of VOCs, *Catalysis Communications* 565 (2014) 134-138, <https://doi.org/10.1016/j.catcom.2014.07.023>.
- [24] V.H. Vu, J. Belkouch, A. Ould-Dris, B. Taouk, Catalytic oxidation of volatile organic compounds on manganese and copper oxides supported on titania, *Reactors, Kinetics, and Catalysis* 54 (2008) 1585-1591, <https://doi.org/10.1002/aic.11482>.
- [25] M.R. Morales, B.P. Barbero, L.E. Cadús, Total oxidation of ethanol and propane over Mn-Cu mixed oxide catalysts, *Applied Catalysis B: Environmental* 67 (2006) 229–236, <https://doi.org/10.1016/j.apcatb.2006.05.006>.
- [26] W. Tang, X. Wu, G. Liu, S. Li, D. Li, W. Li, Y. Chen, Preparation of hierarchical layer-stacking Mn-Ce composite oxide for catalytic total oxidation of VOCs, *Journal of Rare Earths* 33 (2015) 62-69, [https://doi.org/10.1016/S1002-0721\(14\)60384-7](https://doi.org/10.1016/S1002-0721(14)60384-7).
- [27] Y. Luo, D. Lin, Y. Zheng, X. Feng, Q. Chen, K. Zhang, X. Wang, L. Jiang, MnO<sub>2</sub> nanoparticles encapsulated in spheres of Ce-Mn solid solution: Efficient catalyst and good water tolerance for low-temperature toluene oxidation, *Applied Surface Science* 504 (2020) 144481, <https://doi.org/10.1016/j.apsusc.2019.144481>.

- [28] X. Chen, Q. Xu, Y. Zhou, Q. Zhu, H. Huang, Z. Pan, P. Zhang, S. Dai, H. Lu, Facile and Flexible Preparation of Highly Active CuCe Monolithic Catalysts for VOCs Combustion, *Chemistry Select* 2 (2017) 9069-9073, <https://doi.org/10.1002/slct.201701850>.
- [29] Q. Wang, Z. Li, M.A. Bãñares, L.T. Weng, Q. Gu, J. Price, W. Han, K.L. Yeung, A Novel Approach to High-Performance Aliovalent-Substituted Catalysts—2D Bimetallic MOF-Derived CeCuO<sub>x</sub> Microsheets, *Small* 15 (2019) 1903525, <https://doi.org/10.1002/smll.201903525>.
- [30] Y. Dong, J. Zhao, J.Y. Zhang, Y. Chen, X. Yang, W. Song, L. Wei, W. Li, Synergy of Mn and Ni enhanced catalytic performance for toluene combustion over Ni-doped  $\alpha$ -MnO<sub>2</sub> catalysts, *Chemical Engineering Journal* 388 (2020) 124244, <https://doi.org/10.1016/j.cej.2020.124244>.
- [31] H. Xu, N. Yan, Z. Qu, W. Liu, J. Mei, W. Huang, S. Zhao, Gaseous Heterogeneous Catalytic Reactions over Mn-Based Oxides for Environmental Applications: A Critical Review, *Environmental Science & Technology* 51 (2017) 8879–8892, <https://doi.org/10.1021/acs.est.6b06079>.
- [32] S.-C. Jung, Y.-K. Park, H.Y. Jung, U.I. Kang, J.W. Nah, S.C. Kim, Effects of calcination and support on supported manganese catalysts for the catalytic oxidation of toluene as a model of VOCs, *Research on Chemical Intermediates* 42 (2016) 185-199, <https://doi.org/10.1007/s11164-015-2333-6>.
- [33] V.P. Santos, M.F.R. Pereira, J.J.M. Órfãõ, J.L. Figueiredo, The role of lattice oxygen on the activity of manganese oxides towards the oxidation of volatile organic compounds, *Applied Catalysis B: Environmental* 99 (2010) 353-363, <https://doi.org/10.1016/j.apcatb.2010.07.007>.

- [34] S.C. Kim, W.G. Shim, Catalytic combustion of VOCs over a series of manganese oxide catalysts, *Applied Catalysis B: Environmental* 98 (2010) 180-185, <https://doi.org/10.1016/j.apcatb.2010.05.027>.
- [35] Y. Lyu, C. Li, X. Du, Y. Zhu, Y. Zhang, S. Li, Catalytic removal of toluene over manganese oxide-based catalysts: a review, *Environmental Science and Pollution Research* 27 (2020) 2482–2501, <https://doi.org/10.1007/s11356-019-07037-2>.
- [36] H. Cao, X. Li, Y. Chen, M. Gong, J. Wang, Effect of loading content of copper oxides on performance of Mn-Cu mixed oxide catalysts for catalytic combustion of benzene, *Journal of Rare Earths* 30 (2012) 871-877, [https://doi.org/10.1016/S1002-0721\(12\)60148-3](https://doi.org/10.1016/S1002-0721(12)60148-3).
- [37] D.A. Aguilera, A. Perez, R. Molina, S. Moreno, Cu–Mn and Co–Mn catalysts synthesized from hydrotalcites and their use in the oxidation of VOCs, *Applied Catalysis B: Environmental* 104 (2011) 144–150, <https://doi.org/10.1016/j.apcatb.2011.02.019>.
- [38] L. Li, J. Luo, Y. Liu, F. Jing, D. Su, W. Chu, Self-Propagated Flaming Synthesis of Highly Active Layered CuO- $\delta$ -MnO<sub>2</sub> Hybrid Composites for Catalytic Total Oxidation of Toluene Pollutant, *ACS Applied Materials & Interfaces* 9 (2017) 21798–21808, <https://doi.org/10.1021/acsami.7b04380>.
- [39] M. Luo, Y. Cheng, X. Peng, W. Pan, Copper modified manganese oxide with tunnel structure as efficient catalyst for low-temperature catalytic combustion of toluene, *Chemical Engineering Journal* 369 (2019) 758-765, <https://doi.org/10.1016/j.cej.2019.03.056>.
- [40] Z. Xiao, J. Yang, R. Ren, J. Li, N. Wang, W. Chu, Facile synthesis of homogeneous hollow microsphere Cu–Mn based catalysts for catalytic oxidation of toluene, *Chemosphere* 247 (2020) 125812, <https://doi.org/10.1016/j.chemosphere.2020.125812>.
- [41] H. Wang, Y. Lu, Y.X. Han, C. Lu, H. Wan, Z. Xu, S. Zheng, Enhanced catalytic toluene oxidation by interaction between copper oxide and manganese oxide in Cu-O-Mn/ $\gamma$ -

Al<sub>2</sub>O<sub>3</sub> catalysts, *Applied Surface Science* 420 (2017) 260–266, <https://doi.org/10.1016/j.apsusc.2017.05.133>.

[42] S.M. Saqer, D.I. Kondarides, X.E. Verykios, Catalytic oxidation of toluene over binary mixtures of copper, manganese and cerium oxides supported on  $\gamma$ -Al<sub>2</sub>O<sub>3</sub>, *Applied Catalysis B: Environmental* 103 (2011) 275–286, <https://doi.org/10.1016/j.apcatb.2011.01.001>.

[43] S. Behar, P. Gonzalez, P. Agulhon, F. Quignard, D. Świerczyński, New synthesis of nanosized Cu–Mn spinels as efficient oxidation catalysts, *Catalysis Today* 189 (2012), <https://doi.org/10.1016/j.cattod.2012.04.004>.

[44] W.B. Li, M. Zhuang, J.X. Wang, Catalytic combustion of toluene on CuMn/MCM-41 catalysts: Influence of calcination temperature and operating conditions on the catalytic activity, *Catalysis Today* 137 (2008) 340–344, <https://doi.org/10.1016/j.cattod.2007.11.002>.

[45] H.J. Kim, S.W. Choi, C.S. Lee, B. Wielage, S. Bae, S.O. Obare, H.I. Inyang, Oxidation of toluene on  $\gamma$ -Al<sub>2</sub>O<sub>3</sub> supported copper-manganese catalysts, *Environmental Engineering Science* 28 (2011) 827–833, <https://doi.org/10.1089/ees.2010.0116>.

[46] C.A. Emeis, Determination of Integrated Molar Extinction Coefficients for Infrared Absorption Bands of Pyridine Adsorbed on Solid Acid Catalysts, *Journal of Catalysis* 141 (1993) 347–354, <https://doi.org/10.1006/jcat.1993.1145>.

[47] J.B. Higgins, R.B. LaPierre, J.L. Schlenker, A.C. Rohrman, J.D. Wood, G.T. Kerr, W.J. Rohrbaugh, The framework topology of zeolite beta, *Zeolites* 8 (1988) 446–452, [https://doi.org/10.1016/S0144-2449\(88\)80219-7](https://doi.org/10.1016/S0144-2449(88)80219-7).

[48] F. Wang, H. Wu, Z. Lin, S. Han, D. Wang, Y. Xue, Y. Sun, J. Sun, B. Li, Shape evolution of Cu-doped Mn<sub>3</sub>O<sub>4</sub> spinel microcrystals: influence of copper content, *Materials Research Bulletin* 45 (2010) 1567–1573, <https://doi.org/10.1016/j.materresbull.2010.07.022>.

- [49] S. Xiong, Y. Peng, D. Wang, N. Huang, Q. Zhang, S. Yang, J. Chen, J. Li, The role of the Cu dopant on a  $Mn_3O_4$  spinel SCR catalyst: Improvement of low-temperature activity and sulfur resistance, *Chemical Engineering Journal* 387 (2020) 124090, <https://doi.org/10.1016/j.cej.2020.124090>.
- [50] S. Dzwigaj, M.J. Peltre, P. Massiani, A. Davidson, M. Che, T. Sen, S. Sivasanker, Incorporation of vanadium species in a dealuminated  $\beta$  zeolite, *Chemical Communications* (1998) 87-88, <https://doi.org/10.1039/A704556E>.
- [51] S. Dzwigaj, P. Massiani, A. Davidson, M. Che, Role of silanol groups in the incorporation of V in  $\beta$  zeolite, *Journal of Molecular Catalysis A: Chemical* 155 (2000) 169-182, [https://doi.org/10.1016/S1381-1169\(99\)00332-5](https://doi.org/10.1016/S1381-1169(99)00332-5).
- [52] M. Trejda, M. Ziolek, Y. Millot, K. Chalupka, M. Che, S. Dzwigaj, Methanol oxidation on VSiBEA zeolites: Influence of V content on the catalytic properties, *Journal of Catalysis* 281 (2011) 169-176, <https://doi.org/10.1016/j.jcat.2011.04.013>.
- [53] S. Dzwigaj, M. Matsuoka, R. Franck, M. Anpo, M. Che, Probing Different Kinds of Vanadium Species in the VSi $\beta$  Zeolite by Diffuse Reflectance UV–Visible and Photoluminescence Spectroscopies, *Journal of Physical Chemistry B* 102 (1998) 6309-6312, <https://doi.org/10.1021/jp981454+>.
- [54] S. Dzwigaj, M. Matsuoka, R. Franck, M. Anpo, M. Che, Evidence of Three Kinds of Tetrahedral Vanadium (V) Species in VSi $\beta$  Zeolite by Diffuse Reflectance UV–Visible and Photoluminescence Spectroscopies. *Journal of Physical Chemistry B* 104 (2000) 6012-6020, <https://doi.org/10.1021/jp0000331>.
- [55] R. Hajjar, Y. Millot, P.P. Man, M. Che, S. Dzwigaj, Two kinds of framework Al sites studied in BEA zeolite by X-ray diffraction, Fourier Transform Infrared Spectroscopy, NMR techniques, and V probe. *Journal of Physical Chemistry C* 112 (2008) 20167– 20175, [10.1021/jp808356q](https://doi.org/10.1021/jp808356q).

- [56] T. Barzetti, E. Selli, D. Moscotti, L. Forni, Pyridine and ammonia as probes for FTIR analysis of solid acid catalysts, *Journal of the Chemical Society, Faraday Transactions* 92 (1996) 1401-1407, <https://doi.org/10.1039/FT9969201401>.
- [57] J. Niu, H. Liu, H. Qian, J. Liu, M. Ma, E. Duan, L. Yu, Preparation of metal-doped Cu–Mn/HTS-1 catalysts and their mechanisms in efficient degradation of toluene, *Journal of Environmental Sciences* 88 (2020) 260-272, <https://doi.org/10.1016/j.jes.2019.08.019>.
- [58] T. Kondratowicz, M. Drozdek, A. Rokicińska, P. Natkański, M. Michalik, P. Kuśtrowski, Novel CuO-containing catalysts based on ZrO<sub>2</sub> hollow spheres for total oxidation of toluene, *Microporous and Mesoporous Materials* 279 (2019) 446-455, <https://doi.org/10.1016/j.micromeso.2019.01.031>.
- [59] A. Wąskowska, L. Gerward, J. Staun Olsen, S. Steenstrup, E. Talik, CuMn<sub>2</sub>O<sub>4</sub>: properties and the high-pressure induced Jahn–Teller phase transition, *Journal of Physics: Condensed Matter* 13 (2001) 2549-2562, <https://doi.org/10.1088/0953-8984/13/11/311>.
- [60] E.S. Ilton, J.E. Post, P.J. Heaney, F.T. Ling, S.N. Kerisit, XPS determination of Mn oxidation states in Mn (hydr)oxides, *Applied Surface Science* 366 (2016) 475-485, <http://dx.doi.org/10.1016/j.apsusc.2015.12.159>.
- [61] Y. Zhou, X. Liu, K. Wang, J. Li, X. Zhang, X. Jin, X. Tang, X. Zhu, R. Zhang, X. Jiang, B. Liu, Porous Cu-Mn-O catalysts fabricated by spray pyrolysis method for efficient CO oxidation, *Results in Physics* 12 (2019) 1893-1900, <https://doi.org/10.1016/j.rinp.2019.01.049>.
- [62] M.C. Biesinger, Advanced analysis of copper X-ray photoelectron spectra, *Surface and Interface Analysis* 49 (2017) 1325-1334, <https://doi.org/10.1002/sia.6239>.
- [63] J. Papavasiliou, G. Avgouropoulos, T. Ioannides, Combined steam reforming of methanol over Cu-Mn spinel oxide catalysts, *Journal of Catalysis* 251 (2007) 7-20, <http://dx.doi.org/10.1016/j.jcat.2007.07.025>.

- [64] T. Tabakova, E. Kolentsova, D. Dimitrov, K. Ivanov, M. Manzoli, A.M. Venezia, Y. Karakirova, P. Petrova, D. Nihtianova, G. Avdeev, CO and VOCs Catalytic Oxidation Over Alumina Supported Cu–Mn Catalysts: Effect of Au or Ag Deposition, *Topics in Catalysis* 60 (2017) 110-122, <https://doi.org/10.1007/s11244-016-0723-7>.
- [65] X. Yang, X. Yu, M. Lin, X. Ma, M. Ge, Enhancement effect of acid treatment on  $\text{Mn}_2\text{O}_3$  catalyst for toluene oxidation, *Catalysis Today* 327 (2019) 254–261, <https://doi.org/10.1016/j.cattod.2018.04.041>.
- [66] Y. Zhang, Z. Zeng, Y. Li, Y. Hou, J. Hu, Z. Huang, Effect of the A-site cation over spinel  $\text{AMn}_2\text{O}_4$  ( $\text{A} = \text{Cu}^{2+}, \text{Ni}^{2+}, \text{Zn}^{2+}$ ) for toluene combustion: Enhancement of the synergy and the oxygen activation ability, *Fuel* 288 (2021) 119700, <https://doi.org/10.1016/j.fuel.2020.119700>.
- [67] F. Hu, J. Chen, S. Zhao, K. Si, W. Si, H. Song, J. Li, Toluene catalytic combustion over copper modified  $\text{Mn}_{0.5}\text{Ce}_{0.5}\text{O}_x$  solid solution sponge-like structures, *Applied Catalysis A: General* 540 (2017) 57–67, <https://doi.org/10.1016/j.apcata.2017.04.010>.
- [68] X. Liu, Q. Yu, H. Chen, P. Jiang, J. Li, Z. Shen, The promoting effect of S-doping on the  $\text{NH}_3$ -SCR performance of  $\text{MnO}_x/\text{TiO}_2$  catalyst, *Applied Surface Science* 508 (2019) 144694, <https://doi.org/10.1016/j.apsusc.2019.144694>.
- [69] Y. Zhang, C. Li, Y. Zhu, X. Du, Y. Lyu, S. Li, Y. Zhai, Insight into the enhanced performance of toluene removal from simulated flue gas over Mn-Cu oxides modified activated coke, *Fuel* 276 (2020) 118099, <https://doi.org/10.1016/j.fuel.2020.118099>.
- [70] G. Wei, Q. Zhang, D. Zhang, J. Wang, T. Tang, H. Wang, X. Liu, Z. Song, P. Ning, The influence of annealing temperature on copper-manganese catalyst towards the catalytic combustion of toluene: The mechanism study, *Applied Surface Science* 497 (2019) 143777, <https://doi.org/10.1016/j.apsusc.2019.143777>.

[71] C. Dong, Z. Qu, X. Jiang, Y. Ren, Tuning oxygen vacancy concentration of MnO<sub>2</sub> through metal doping for improved toluene oxidation, *Journal of Hazardous Materials* 391 (2020) 122181, <https://doi.org/10.1016/j.jhazmat.2020.122181>.

[72] H.C. Genuino, S. Dharmarathna, E.C. Njagi, M.C. Mei, S.L. Suib, Gas-Phase Total Oxidation of Benzene, Toluene, Ethylbenzene, and Xylenes Using Shape-Selective Manganese Oxide and Copper Manganese Oxide Catalysts, *Journal of Physical Chemistry C* 116 (2012) 12066-12078, <https://doi.org/10.1021/jp301342f>.